Chapter 1

Introduction

1.1 Scientific Objective

Intermediate waters in the oceans (∼500 to 1000 metres below sea level (mbsl)) make up a global volume of 0.385 x $10^{18} m^3$ (*Talley*, 1999) and are implicated as playing a major role in global ocean circulation (*Schmitz*, 1995). Our knowledge of their formation mechanisms, circulation paths and mixing with other water masses in the oceans is poorly understood. Recent evidence from deep sea cores (*Spero and Lea*, 2002) and modelling (*Saenko et al.*, 2003) also suggests that the intermediate waters may play a crucial role during global climate transitions.

The first objective, and part, of this thesis is to use modern ocean geochemical datasets to ascertain the present circulation and distribution of intermediate water masses in the Pacific. The study focusses specifically on Antarctic Intermediate Water (AAIW) in the Coral Sea and Tasman Sea in the southwest Pacific. The second objective, and part, of this thesis is to utilize results from marine sediment cores taken from the Capricorn Channel, southern Great Barrier Reef, to determine changes in ocean circulation during the Late Quaternary. This will provide insight into the glacial/interglacial evolution of circulation patterns in the intermediate and surface waters of the Coral Sea and Tasman Sea, which can be correlated to local and global climate change.

Carbon isotopes, alkalinity and total inorganic carbon are used as geochemical traces to study the intermediate water masses, but they are also useful to understand the present carbon cycle. Carbon isotopes are also one of the few tracers that can be measured directly from foraminiferal carbonate to provide evidence of changes in the partitioning between carbon reservoirs in the past. The carbon cycle is intrinsically linked to climate through a number of feedback loops, many of which are not well understood. This study is specifically aimed at the present and past. By understanding the impact of changes in the carbon cycle on climate in the recent geological past, and monitoring the present oceans, atmosphere, and terrestrial biosphere, better models can be constructed to enable predictions of future climate change, such as those predicted by the Intergovernmental Panel on Climate Change Report (*Intergovernmental Panel on Climate Change (IPCC)*,

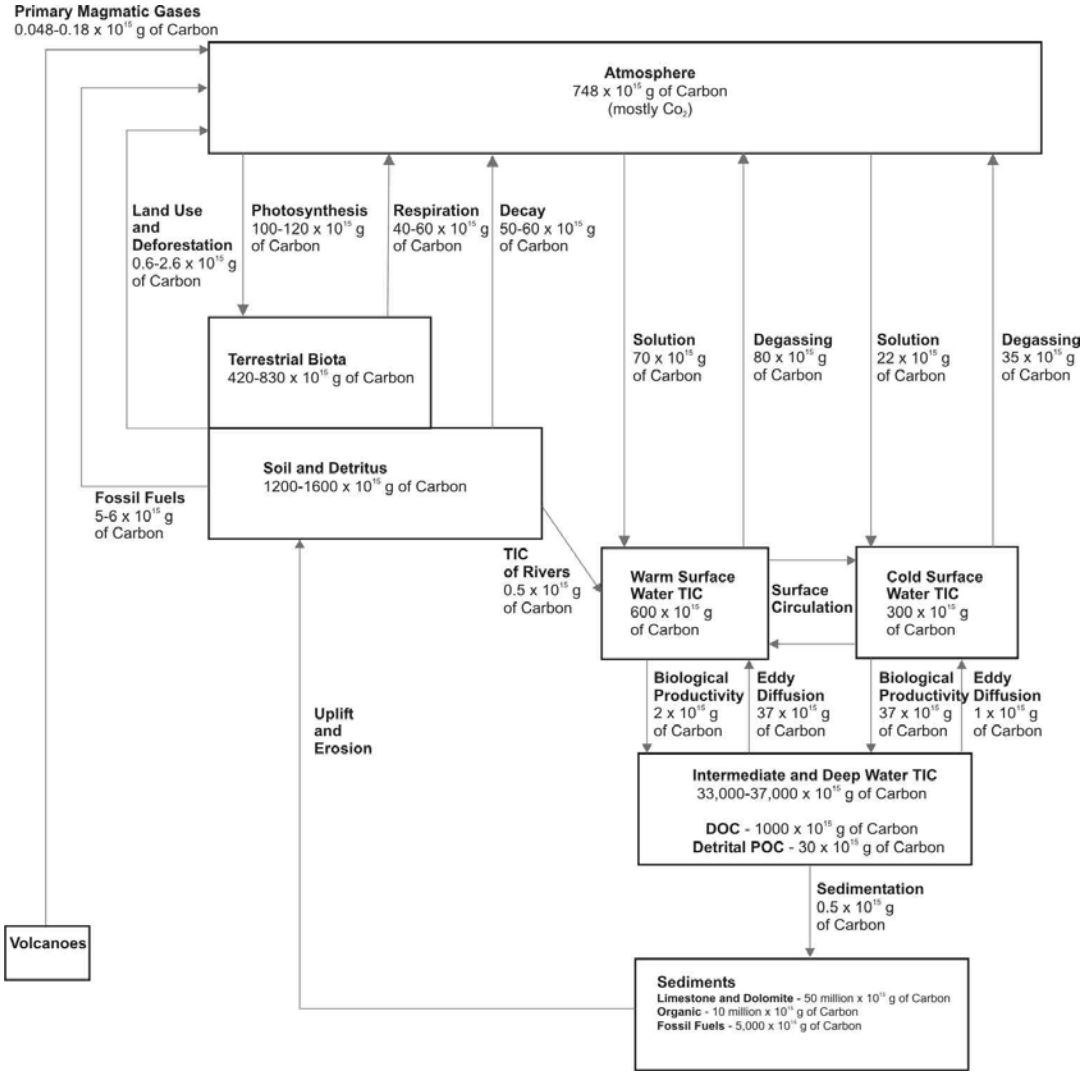

Figure 1.1: The biogeochemical cycle of carbon. Current anthropogenically influenced estimates of the major reservoirs and fluxes per year. Adapted from *Libes* (1992).

1990, 1992).

1.2 Carbon Cycle and Geochemistry

Carbon exchanges between the geosphere, biosphere, atmosphere and oceans. Over millions of years, the geosphere modulates atmospheric CO_2 concentration. At intermediate timescales, (i.e. 10^3 years), however, the oceans play a primary role in regulating and storing CO_2. The oceans store 50 to 60 times more carbon than the atmosphere at present (Figure 1.1) and there is considerable annual exchange between the oceans, atmosphere and biosphere. There are large uncertainties in the size of some of the estimated fluxes, and some of these fluxes have changed considerably as a result of recent anthropogenic influences (Figure 1.1).

Public and scientific interest in the carbon cycle has increased as a result of rapidly

rising concentrations of atmospheric CO_2 caused by anthropogenic activities. Since direct measurements began in 1957, atmospheric CO_2 has risen from ~315 ppmv to ~356 ppmv, by 1993. Evidence from tree ring records show that atmospheric CO_2 was ~280 ppmv in the 1800's, which indicates that human activities over the last two centuries have contributed to a ~76 ppmv rise in atmospheric concentrations. The main culprits of this increase are: the clearing of land, and associated change in terrestrial biomass, and fossil fuel combustion. This has been slightly offset by CO_2 fertilisation of plants, the regrowth of high latitude forests and more absorption of CO_2 in the oceans. Accounting for all the sources and sinks of the increasing atmospheric CO_2 is still problematic ("The Missing Sink" - *Wigley and Schimel* (2000)).

1.2.1 Ice Core Records and Atmospheric CO_2

A variety of information has been used to extend the atmospheric CO_2 record into the recent geological past. These data sets have been used to understand natural variations in the concentrations of atmospheric CO_2 and associated climate change.

The best records for the late Quaternary come from direct measurement of atmospheric CO_2 concentrations of air trapped in ice cores. Other gases, such as CH_4, O_2, N_2O, can also be measured, along with a range of isotopes within the trapped air and ice.

Antarctic ice cores records of gases stretch back to 426 ka, over four glacial cycles (*Petit et al.*, 1997), and recently extracted Antarctic ice cores collected during the EPICA project may extend this record back to almost 740 ka (*EPICA community members*, 2004). These records, and similar ice core records from Greenland (GRIP and GISP2), have revolutionised our understanding of palaeoclimate in the Quaternary. Correlations have been made between ice cores from Greenland and Antarctica to compare the timing of events in the Northern and Southern Hemisphere. Leads and lags between increases or decreases in gases, dust, acid concentrations, isotopes (oxygen) and temperature (determined from deuterium isotope analysis) help to determine the exact sequence of events and possible forcing and feedback mechanisms in the climate system (*Sowers and Bender*, 1995; *Blunier et al.*, 1998; *Broecker and Henderson*, 1998; *Alley*, 2000; *Pepin et al.*, 2001; *Steig and Alley*, 2002; *Caillon et al.*, 2003).

During Termination I, the last glacial/interglacial transition, the rise in temperatures is closely followed by the rapid release of CO_2, and other greenhouse gases such as CH_4. These greenhouse gases cause a positive feedback in the climate system, further increasing temperatures and initiating the melting of the ice sheets and subsequent rising of sea level. Our understanding of these natural feedbacks is far from comprehensive, and although it is assumed that the excess carbon is stored in the deep oceans during glacial periods, there is a lack of suitable evidence or mechanisms for its drawdown and storage. 1.1). The rapid rise in atmospheric CO_2 during early deglaciations (Figure 1.2) highlights the potential role of CO_2 in the climate system. The rapid increase in atmospheric CO_2 (over a few thousand years), requires a significant exchange of CO_2 between the ocean and atmosphere, as the biosphere reservoir of carbon is not large enough to account for this

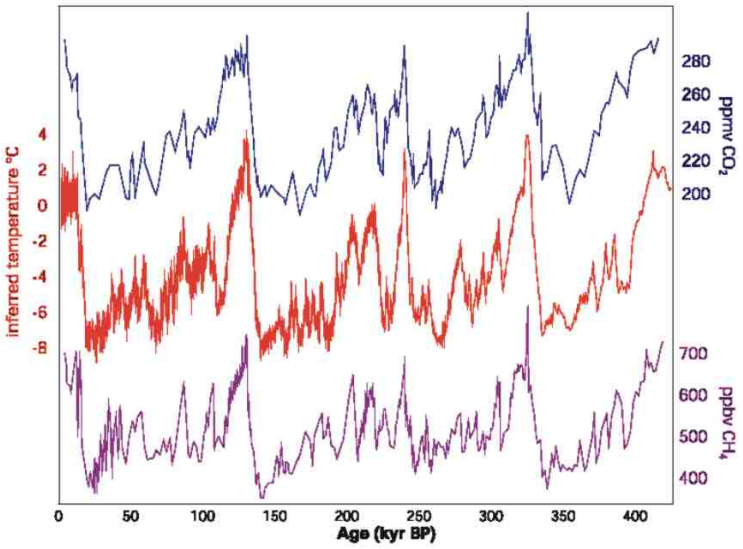

Figure 1.2: Records of CO_2, CH_4 and deuterium (as a proxy for temperature) for the last 400 kyr from the Vostok ice core record (*Petit et al.*, 1999). The 100 kyr glacial/ interglacial cycles and the close correlation between CO_2, CH_4 and temperature are clearly evident.

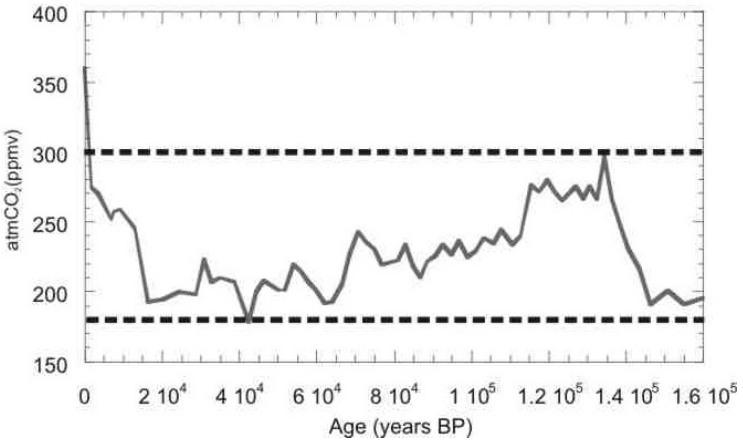

Figure 1.3: Atmospheric CO_2 concentrations measured from the Vostok ice core (*Barnola et al.*, 1987) for the last 150 kyr and direct measurements for the last 50 years. The dashed lines show the natural limits of the glacial/interglacial range in atmospheric CO_2. The present rise in anthropogenic atmospheric CO_2 exceeds this natural range.

change (*Broecker and Peng*, 1982)(Figure 1.1).

1.2.2 Carbon Chemistry of the Oceans

Atmospheric CO_2 concentrations are in equilibrium with CO_2 in the ocean surface waters due to rapid exchange across the air-sea interface. This exchange is controlled by a number of factors such as: the partial pressure of atmospheric CO_2 (pCO_2), the sea surface temperature (SST), and wind mixing of surface waters (*Wanninkhof and Thoning*, 1993).

Once the CO_2 is in solution, however, it rapidly equilibrates with bicarbonate (HCO_3^-) and carbonate (CO_3^{2-}) ions in the water.

$$\begin{aligned} CO_2(g) &\rightleftharpoons CO_2(aq) \\ CO_2(aq) + H_2O &\rightleftharpoons H_2CO_3 \\ H_2CO_3 &\rightleftharpoons H^+ + HCO_3^- \\ HCO_3^- &\rightleftharpoons H^+ + CO_3^{2-} \end{aligned}$$

The carbon species in seawater are used to form solid material. CO_2(g) is used by photosynthetic organisms in the surface layer of the oceans to form organic matter, whilst the bicarbonate is used to produce skeletal carbonate (*Ware et al.*, 1991).

$$\begin{aligned} CO_2(g) + H_2O &\rightleftharpoons CH_2O + O_2 \\ Ca^{2+} + 2HCO_3^- &\rightleftharpoons CaCO_3 + CO_2 + H_2O \end{aligned}$$

The majority of carbon in seawater is in the form of bicarbonate at the pH of seawater (pH 7-8.5). Carbon, as a result of its ability to exist as ions of different charges, acts as an effective pH buffer. The amount of dissolved CO_2 gas in seawater is very small and usually ignored. Therefore, it is the ratio between CO_3^{2-} and HCO_3^- that is important in balancing the electrical charge in the ocean and maintaining pH.

Many ions collectively make up the electrical charge of the ocean. The major cations are Na^+, K^+, Mg^{2+}, and Ca^{2+}. To determine the total charge, it is necessary to multiply the number of moles/kg of each cation by its charge. This provides about 0.606 equivalents of positive charge per kg of seawater. The major anions present in seawater include Cl^-, SO_4^{2-}, Br^-, CO_3^{2-} and HCO_3^-. Without the contribution of CO_3^{2-} and HCO_3^-, the other anions only contribute 0.604 equivalents of negative charge per kg. This leaves a difference of 0.002, made up primarily of CO_3^{2-} and HCO_3^-. The ratio between these two ions depends on the charge required to balance the cations, as the total amount of carbon cannot change. (Note that $B(OH)_3$ and $B(OH)_4^-$ are also present and require a slight correction.) Alkalinity is the measure of the CO_3^{2-} and HCO_3^- charge present to balance the excess positive charge (*Broecker and Peng*, 1982).

Total Inorganic Carbon (TIC) is the measure of the total amount of carbonate and bicarbonate ions present. To determine how the carbonate ion content varies in seawater requires the measurement of the alkalinity and the TIC. (For more details on alkalinity and TIC refer to Appendix A)

$$\begin{aligned} Alkalinity &= 2[CO_3^{2-}] + [HCO_3^-] \\ Total\ \ Inorganic\ \ Carbon\ \ (TIC) &= [CO_3^{2-}] + [HCO_3^-] \end{aligned}$$

$$\begin{aligned} Alk - TIC &= [CO_3^{2-}] \\ 2 * TIC - Alk &= [HCO_3^-] \end{aligned}$$

The formation of organic matter affects the TIC, but has no bearing on the alkalinity. The removal of carbon for skeletal carbonate formation, however, affects both the alkalinity and the TIC. When $CaCO_3$ is formed it decreases the alkalinity by twice as much as the TIC as it removes Ca^{2+} and therefore removes two negative charges in order to maintain electrical neutrality. Alkalinity and TIC in the oceans are consequently related to the pH, as well as the partial pressure of CO_2. Measurements of any two of these four parameters can be used to calculate the others. They can also be used to calculate the saturation states of aragonite and calcite which are directly correlated to HCO_3^- and CO_3^{2-} concentrations (refer to Appendix A).

Organic matter is fixed in surface waters by phytoplankton. Once the organisms expire, they sink through the water column and the organic matter is remineralised, consuming oxygen in the process. This releases carbon and nutrients back into the deep-waters. Organic matter is composed of carbon, nitrogen, phosphorous and oxygen with an average atomic ratio of C:N:P:O = 106:16:1:138 (the so called Redfield Ratio (*Redfield*, 1958). The equation of photosynthesis is from left to right, and for remineralisation right to left.

$$106CO_2 + 16HNO_3 + H_3PO_4 + 122H_2O \rightleftharpoons CH_2O_{106}(NH_3)_{16}H_3PO_4 + 138O_2$$

The oceanic reservoirs of nitrogen and phosphorous are small. They are rapidly removed from the surface waters in most of the global ocean (with the exception of high latitudes), therefore they are usually biolimiting nutrients in the photic zone. The distribution of these elements is primarily controlled by biologically mediated redox processes that drive the bio-geochemical cycles of organic matter, and also by ocean circulation.

1.2.3 Stable and Radioactive Isotopes

Many elements in the oceans have a range of measurable isotopes. The stable isotopes of carbon and oxygen, and radioactive carbon are commonly used as oceanographic and palaeoceanographic tracers. Carbon has three main isotopes: ^{12}C - 98.9%, ^{13}C - 1.1% and ^{14}C - 10^{-10}%. The first two are stable isotopes, while ^{14}C is radioactive with a half life of 5730 years. Oxygen also has three stable isotopes: ^{16}O - 99.8%, ^{17}O - 0.04% and ^{18}O - 0.2%. Usually ^{17}O is ignored in palaeoceanographic research due to its low abundance.

Stable Carbon Isotopes

Plants preferentially use ^{12}C during photosynthesis, which alters the ratio of carbon isotopes left in the atmosphere and surface oceans. The ratio of $^{13}C/^{12}C$ is often measured to study variations in biological productivity. This ratio is determined by the equation below and is denoted as $\delta^{13}C‰$.

$$\delta^{13}C = \frac{(^{13}C/^{12}C_{sample} - ^{13}C/^{12}C_{std})}{(^{13}C/^{12}C_{std} - 1)} * 1000$$

where the standard commonly used is the Vienna Pee Dee Belemite (VPDB).

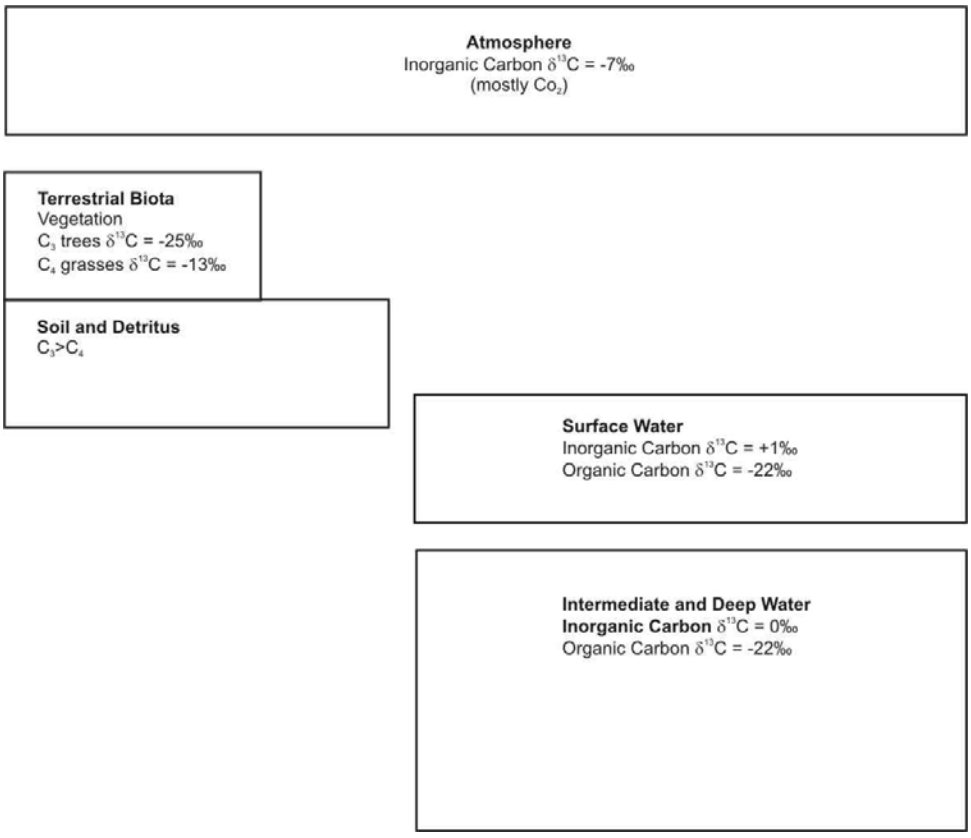

Figure 1.4: The natural $\delta^{13}C$ values for vegetation, soil, atmospheric CO_2, and organic and inorganic carbon in the oceans. The $\delta^{13}C$ values change if there is increased biological productivity, or a change in the ocean circulation.

The modern average $\delta^{13}C$ values for inorganic and organic carbon within different reservoirs are shown in Figure 1.4. These $\delta^{13}C$ ratios, however, vary spatially and temporally throughout the oceans, atmosphere and biosphere. In the oceans, the spatial and temporal variations in $\delta^{13}C$ are related to three major factors listed below and highlighted in Figure 1.5.

- **Air-sea exchange:** ^{13}C-enrichment of dissolved CO_2 in surface seawater results from the temperature-dependent fractionation of $^{13}C/^{12}C$ during the exchange of CO_2 at the air-sea interface (*Mook et al.*, 1974). Gas exchange rates depend on wind driven mixing in the surface ocean with stronger winds increasing the ^{13}C of seawater. Due to substantial exchange of CO_2 between the atmosphere and the cold surface waters of the Southern Ocean, the present-day AAIW has a lower $\delta^{13}C$ (by $\sim$1‰) than would be expected on the basis of its nutrient content and biological productivity (*Oppo and Fairbanks*, 1989; *Charles and Fairbanks*, 1990; *Ninneman and Charles*, 1997).

- **Biological activity:** Primary production of organic carbon preferentially removes ^{12}C from the photic zone (*Kroopnick*, 1985), leaving surface waters enriched in ^{13}C. This is the fundamental cause of the well-known inverse relationship between $\delta^{13}C$

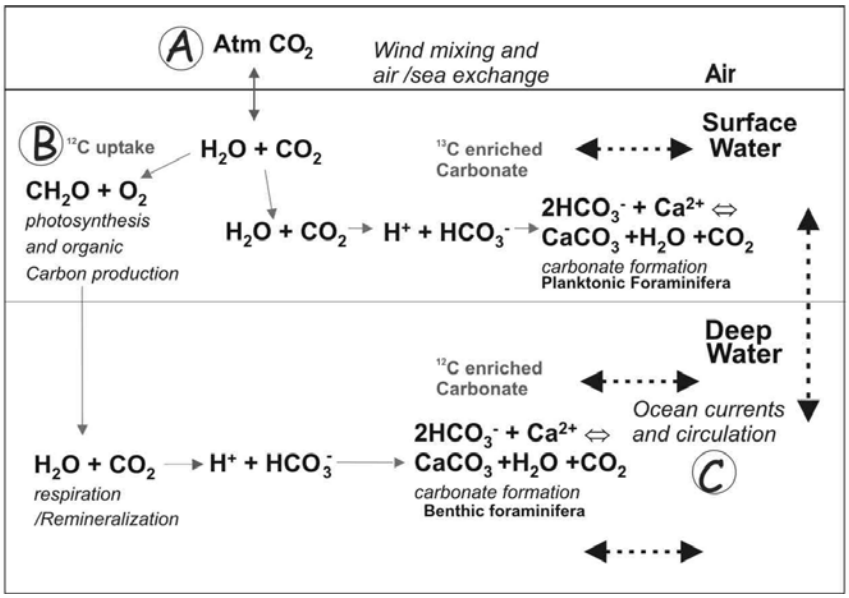

Figure 1.5: The three major factors that affect the $\delta^{13}C$ of the oceans ; **A**: Air-Sea exchange, **B**: Biological productivity and **C**: Ocean Circulation. Adapted from (*Rohling and Cooke*, 1999) and Cooke (1999))

and nutrient concentrations (e.g. PO_4^{3-}) in the water column (*Broecker and Peng*, 1982). As the particulate organic carbon sinks, it is remineralised via respiration and metabolism, causing the intermediate and deep waters to become enriched in ^{12}C. Given no other influences, this will eventually produce a negative $\delta^{13}C$ gradient between the surface and deep waters.

- **Ocean circulation:** Horizontal and vertical mixing, and the advection of waters of different ^{13}C composition from a range of depths and regions (e.g. upwelling of deeper ^{12}C-enriched waters) can remove or reduce the $\delta^{13}C$ gradient formed by the biological activity.

The $\delta^{13}C$ profiles in the oceans are primarily controlled by biological productivity. Changes to the expected surface to deep $\delta^{13}C$ gradient can be utilised to study variations in the air-sea exchange and ocean circulation. It is important to understand the present day distribution of $\delta^{13}C$ in the oceans as it is one of the few tracers that can be directly measured from the skeletal carbonate of foraminifera preserved in marine sediment cores. It has been widely used to study variations in ocean circulation and changes in the oceanic carbon cycle in the geological past.

Radiocarbon

The radioactive isotope ^{14}C has been widely used as a tracer in oceanography and palaeoceanography. Radiocarbon measurements from modern seawater are very useful as conservative water tracers, whilst ^{14}C measurements on foraminiferal carbonate are useful for dating marine sediment cores over the last 40,000 years.

Measurements of the $\Delta^{14}C$ of TIC made during GEOSECS (Geochemical Oceans Sections Study) allowed confirmation of the theory of the thermohaline conveyor belt deep circulation of the oceans (*Broecker et al.*, 1980). The youngest deep waters are located in the North Atlantic Ocean, and become progressively older through the South Atlantic, Indian Ocean, South Pacific, with the oldest waters of ∼2000 years found in the North Pacific. Combined measurements of benthic and planktonic species can also provide an estimate of changes in ventilation rates of the deep water in the oceans in the past (e.g., *Shackleton et al.* (1988)).

Radiocarbon is a cosmogenic isotope that is formed by the action of cosmic ray neutrons on ^{14}N in the upper atmosphere to produce ^{14}C. The ^{14}C is rapidly distributed throughout the atmosphere in the form of $^{14}CO_2$. All living organisms in equilibrium with the atmosphere incorporate and maintain a natural concentration within their tissues. When an organism dies it can no longer exchange carbon with the atmosphere and initial concentration of ^{14}C begins to decrease due to radioactive decay. Given a half life of 5730 years, and measuring the present concentration it is possible to calculate the age since the organism died and was last in equilibrium with the atmosphere. With the present accelerator mass spectrometry (AMS) techniques, ages can be determined from 200->40,000 years.

The flux of cosmic rays to the atmosphere, however, is not constant and varies as a result of solar activity and geomagnetic modulation (*Stuiver and Quay*, 1980). An increase in sunspot activity and increasing geomagnetic field intensity leads to a reduction in the influx of galactic cosmic rays and results in a decrease in ^{14}C production rates. Consequently, the concentration of ^{14}C has not been uniform in the atmosphere through time, and these fluctuations must be corrected for when the radiocarbon age is calibrated to a calendar age. A number of calibration databases have been produced to do this, including Intcal 98 and Marine 98 (*Stuiver et al.*, 1998). The existing calibration curves are only accurate to 20,000 years. New calibration databases are presently being compiled to extend this further (*Bard et al.*, 2004). Most ages beyond 20,000 years currently use a polynomial calibration curve based on U/Th ages paired with ^{14}C in corals (*Bard*, 1998) .

An additional problem with the use of radiocarbon measurements in the ocean is that the ocean is not in complete equilibrium with the atmosphere. The ^{14}C composition in the surface waters of the ocean is affected by exchange with the atmospheric ^{14}C and mixing from older, upwelling, deeper waters. The ^{14}C concentration in these deeper waters depends on the time since they were last at the surface and the distribution of deep-water masses by bottom currents. The deep-water ^{14}C age for the Atlantic Ocean and Indian Ocean is ∼250 years, whilst for the Pacific Ocean it is closer to 500 years (*Stuiver and Reimer*, 1993). The so called "Reservoir Effect" results in ^{14}C samples providing an age that is greater than expected. The reservoir effect can be determined and corrected for by measuring the $\Delta^{14}C$ of living organisms from a particular location and determining their radiocarbon age. The average reservoir age for the present day surface waters of the oceans is ∼400 years.

$$\text{Reservoir Age} = {}^{14}C_{marinesample} - {}^{14}C_{atmosphere} \text{ at time } t.$$

Several extra corrections are also required to take into account anthropogenic perturbations that have altered the present atmospheric $^{14}C/^{12}C$ ratio and consequently influenced the reservoir age of the surface oceans. The "Suess Effect" is the result of burning fossil fuels, which contain no ^{14}C as they are older than 40,000 years, and causes the dilution of the $^{14}C/^{12}C$ ratio. The second correction is the "Bomb Effect", which is the result of exploding nuclear weapons in the atmosphere between 1955 and 1966. These nuclear explosions released large amounts of ^{14}C into the atmosphere, doubling the $^{14}C/^{12}C$ ratio by 1966.

Oxygen Isotopes

The $^{18}O/^{16}O$ ratio is usually reported as $\delta^{18}O‰$ (similar to the $\delta^{13}C$ and using the same standard). $\delta^{18}O$ is primarily affected by thermodynamic fractionation, where the lighter isotope ^{16}O is favoured in the gaseous state over the heavier ^{18}O, as less energy is required to maintain it as a gas. At higher temperatures, this fractionation between the two isotopes is reduced, as the isotopic mass difference is insignificant compared to the energy level.

The distribution of $\delta^{18}O$ in the oceans is primarily controlled by evaporation and precipitation. This is related to the fact that ^{16}O is more easily evaporated. ^{16}O then precipitates as snow and ice, leaving the oceans enriched in ^{18}O. During the last glacial maximum (LGM) the ice caps of Greenland and Antarctica had $\delta^{18}O$ values of -35 to -50‰ (SMOW - Standard Mean Ocean Water), whilst to compensate for this change in ice volume the oceans exhibit values of +1‰ above the present value of 0‰ (*Schrag et al.*, 2002).

The change in $\delta^{18}O$ of the oceans related to ice volume can be measured in calcitic foraminifera from marine sediment cores. Such records clearly show the asymmetric glacial/ interglacial cycles of approximately 100,000 years. These $\delta^{18}O$ cycles from marine cores have been matched to the Milankovitch cycle of eccentricity (*Milankovitch*, 1941; *Emiliani*, 1955, 1966). Spectral analysis of the $\delta^{18}O$ marine record for the last 400,000 years, highlight shorter cycles of 19,000 to 23,000 years and 41,000 years, which are associated with the insolation forcing of precession and obliquity. These Milankovitch cycles modulate the solar radiation reaching Earth. The Milankovitch forcing of the marine records is more evident in these shorter cycles in contrast with the lack of correspondence between the direct eccentricity forcing and the climate system response (*Imbrie et al.*, 1993). Therefore there must be significant amplification of this 100,000 year signal through feedbacks in the climate system. The $\delta^{18}O$ cycles measured in foraminifera can be tuned to the Milankovitch orbital forcing (*Martinson et al.*, 1987) (Figure 1.6), and this is commonly used to determine an initial chronology for sedimentary marine cores.

The $\delta^{18}O$ measured in carbonate is also related to salinity, temperature and ice volume. Salinity is directly related to changes $\delta^{18}O$, in a very similar manner to ice volume. Salinity related $\delta^{18}O$ is a result of the balance between as precipitation and evaporation.

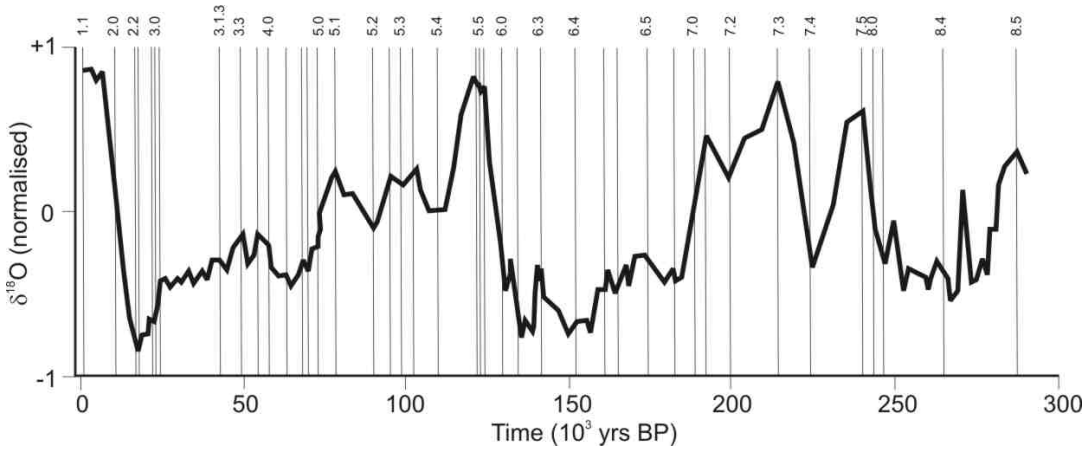

Figure 1.6: The orbitally tuned stacked benthic foraminifera $\delta^{18}O$ SPECMAP curve, with marine isotope stages labelled along the top. Error range is ±5000 years. (*Martinson et al.*, 1987)

Precipitation has a lower $^{18}O/^{16}O$ ratio than seawater and high evaporation results in a higher ratio in seawater. This ratio changes with latitude, with the highest fractionation, and subsequent lowest ratio, at higher latitudes. Close to the coast river discharge can have a large influence on local salinity and $\delta^{18}O$.

The $\delta^{18}O$ of calcite is inversely related to temperature as a result of kinetic processes. At low temperatures the formation rate of carbonate is slower and more selective. This results in the preferential selection of ^{18}O over ^{16}O, despite the fact that ^{18}O is larger and requires more energy to form bonds. However, the resulting covalent bond between carbon and ^{18}O is more stable than the bond formed between carbon and ^{16}O. As temperature rises the formation rate of carbonate increases and becomes less selective, resulting in reduced fractionation between the two isotopes.

Any residual in the $\delta^{18}O$ in carbonate, after ice volume has been accounted for, must reflect local changes in temperature and salinity. Changes in SSTs at the LGM have been highly debated over the last 20 years since the original CLIMAP (Climate: Long range Investigations, Mapping and Prediction estimates (*CLIMAP*, 1976, 1981). The original SST estimates used planktonic foraminifera transfer functions. More recently Modern Analog Techniques (MAT) have also been used and are more accurate, with the compilation of regional databases for planktonic foraminifera e.g., AUSMAT-F2, (*Barrows et al.*, 2000).

Over the last ten years, a range of new geochemical proxies for SSTs have been developed including $Sr : Ca$ of coralline aragonite, $Mg : Ca$ of foraminiferal calcite and U_k^{37} from alkenones. Results from these techniques, along with traditional approaches, still give a wide range of SSTs for the tropics, although they are converging in some places (*Gagan et al.*, 2004). Once it is possible to accurately separate the temperature effect from the $\delta^{18}O$, it will be possible to determine local changes in salinity. Changes in $\delta^{18}O$, which reflect variations in temperature and salinity, can also give an indication of past changes in surface water and atmospheric circulation.

Acronym	Full Name
AABW	Antarctic Bottom Water
AAIW	Antarctic Intermediate Water
AASW	Antarctic Surface Water
ACC	Antarctic Circumpolar Current
CPDW	Circumpolar Deep Water
CTD	Conductivity, temperature, depth profile
EAC	East Australian Current
EEP	Eastern Equatorial Pacific
ENSO	El Niño Southern Oscillation
EUC	Equatorial Undercurrent
IPWP	Indo-Pacific Warm Pool
ITCZ	Inter Tropical Convergence Zone
NADW	North Atlantic Deep Water
NEC	North Equatorial Current
NECC	North Equatorial Counter Current
NGCUC	New Guinea Coastal Undercurrent
NPIW	North Pacific Intermediate Water
PDW	Pacific Deep Water
PF	Polar Front
SAF	Subantarctic Front
SAMW	Subantarctic Mode Water
SEC	South Equatorial Current
SPC	South Pacific Current
STC	Subtropical Convergence (sometimes termed STF - Subtropical Front)
TF	Tasman Front
T-S	potential Temperature v Salinity
WBC	Western Boundary Current

Table 1.1: Oceanography acronyms, see also Appendix G.

1.3 Oceanography

1.3.1 Oceanography of the Pacific Ocean

The Pacific Ocean is the largest of the ocean basins. It covers 178 x 10^6 km^2 including all its adjacent seas, which represents 40% of the surface area of the worlds oceans (*Tomczak and Godfrey*, 1994). The Pacific is made up of a series of basins which result in a more complex bathymetry than the Atlantic Ocean and Indian Ocean (Figure 1.7). The ridges separating the basins restrict deep-water flow between the basins, especially between the Southern Ocean and the south Pacific.

The Pacific Ocean is important, not only because of its immense size, but it also has a significant influence on modern global climate. This is especially evident from the global impacts of El Niño events associated with the Indo-Pacific Warm Pool (IPWP) (Figure 1.8). The El Niño southern oscillation (ENSO) causes a shift in the atmospheric circulation, resulting in a weakening of the equatorial trade winds. This weakening of the trade winds affects the surface currents of the oceans and the local terrestrial climates modulated by these currents. It also influences the convergence and upwelling along the equator and consequently the productivity in the tropics. This is especially true for the high productivity region of the eastern equatorial Pacific (EEP) where ENSO was first

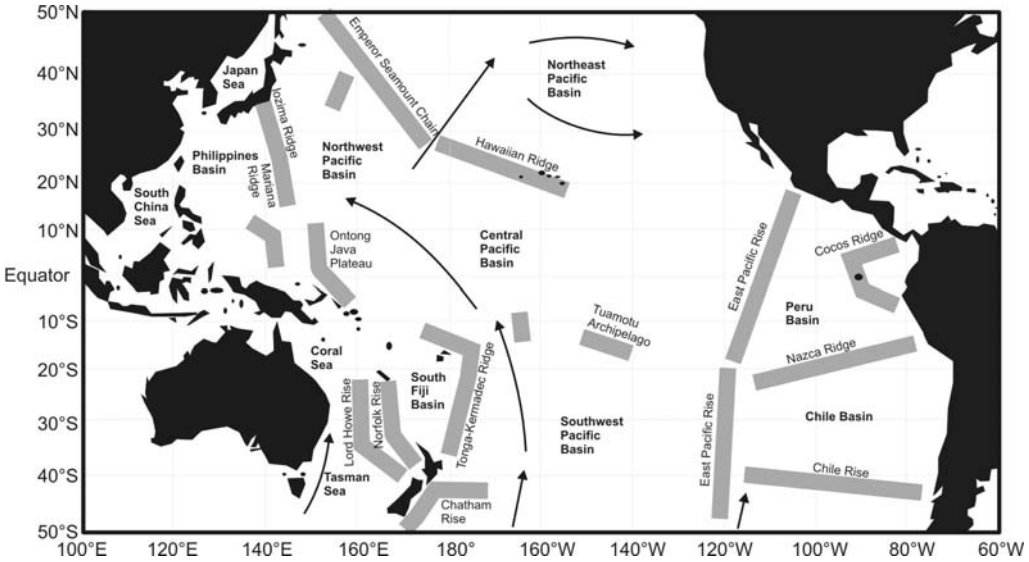

Figure 1.7: Schematic diagram of the topographic barriers (thick grey lines) which divide the Pacific Ocean into a series of basins. The arrows show the circulation of the Antarctic Bottom Waters (AABW) which enters from the Southern Ocean and slowly circulate around some of the Pacific Basins. Many regions of the Pacific are topographically blocked from this AABW circulation. Adapted from *Tomczak and Godfrey* (1994).

recognised and acquired its name. As a result, many palaeoceanographic and palaeoclimate studies have concentrated on the EEP (*Mix et al.*, 1991; *Loubere*, 2001, 2000; *Koutavas et al.*, 2002; *Feldberg and Mix*, 2003; *Koutavas and Lynch-Stieglitz*, 2003; *Spero et al.*, 2003).

Atmospheric circulation influences most of the surface currents in the north and south Pacific gyres. In the equatorial Pacific, the variation in the land-sea temperature difference in the Northern and Southern Hemisphere results in the latitudinal annual displacement of the equatorial trade winds, which affects the position of the intertropical convergence zone (ITCZ) (Figure 1.8). This displacement of the ITCZ is the basis for the annual shift between the southeast Asian monsoon (July-Sep) and the northwest Australasian monsoon (Dec-Feb). These monsoonal systems are intrinsically linked to the IPWP (Figure 1.8). Therefore, the strength of the monsoon today is also influenced by ENSO (*Sen Roy et al.* (2003); *Kawamura et al.* (2003) and many others).

Wind driven models, using the dynamics of *Sverdrup* (1947) and *Munk* (1950), can explain the majority of surface currents in the Pacific Ocean, implying that the surface currents are primarily driven by the wind stress field (Figure 1.9). The equatorial trade winds and the subtropical westerlies define the boundaries of the subtropical ocean gyres north and south of the equator. The northern trade winds are a dominant feature and as a result the Northern Hemisphere subtropical gyre exhibits much stronger circulation than the Southern Hemisphere. The Northern Hemisphere subtropical gyre includes the North Equatorial Current (NEC) centred on 15°N, the Philippines current, the Kuroshio, the North Pacific Current and the California Current (Figure 1.8). The weaker Southern Hemisphere subtropical gyre is defined by the South Equatorial Current (SEC), the East

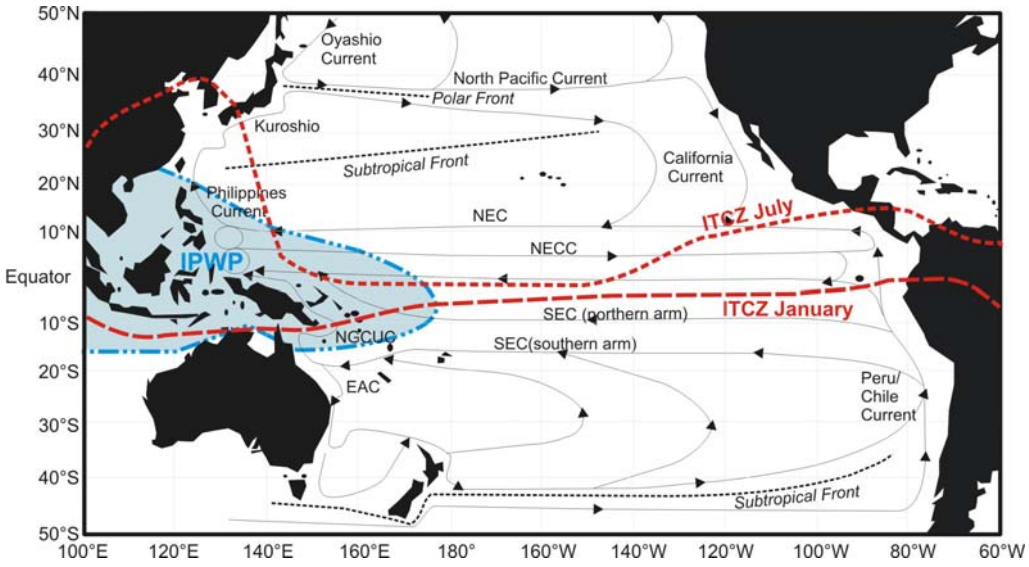

Figure 1.8: Schematic diagram of surface currents of the Northern and Southern Hemisphere subtropical gyres of the Pacific. South Equatorial Current (SEC), North Equatorial Current (NEC), North Equatorial Counter Current (NECC), East Australian Current (EAC) and New Guinea Coastal Undercurrent (NGCUC). The location of the Intertropical Convergence Zone (ITCZ) is shown in red for July (short dashes) and January (long dashes), and the average area covered by he Indo-Pacific Warm Pool (IPWP) is also highlighted in light blue. Adapted from *Tomczak and Godfrey* (1994).

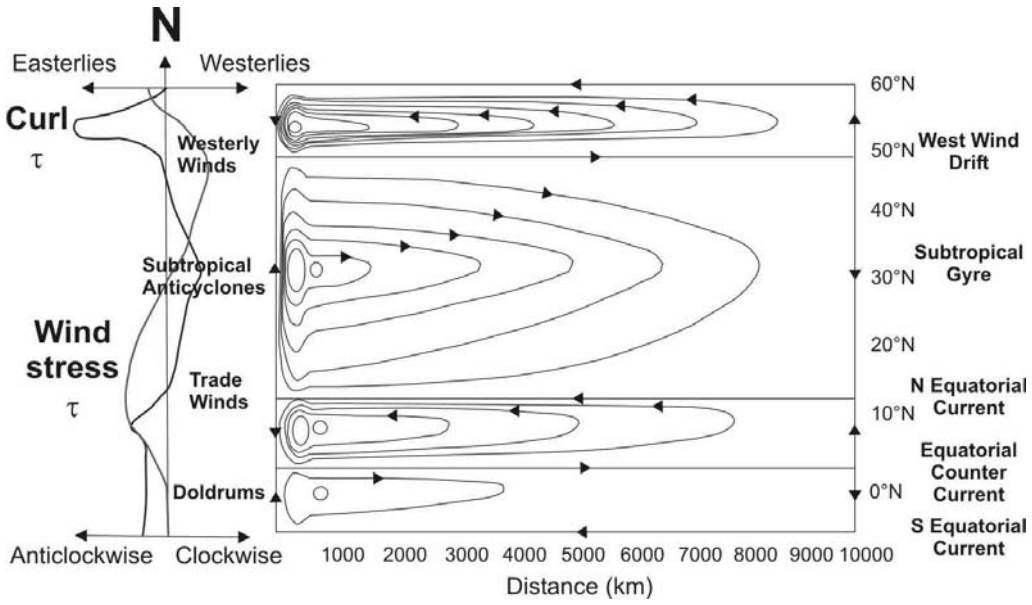

Figure 1.9: Schematic diagram of average annual wind stress τ and curl τ for the northern subtropical gyre of the Atlantic or Pacific and the associated surface ocean circulation (adapted from *Bearman* (1989)). When Wind stress τ is a maximum or minimum, flow is zonal (east-west) and by definition, curl τ is at a maximum at those latitudes where wind stress curve show the greatest change with latitude. At this maximum curl τ transport is meridional, (either southwards or northwards). After *Munk* (1950).

Australian Current (EAC) and the Peru/Chile Current (Figure 1.8). Some of the water from the SEC spills over across the equator east of Papua New Guinea into the northern subtropical gyre system. These surface water currents can be split into western boundary currents (WBC), eastern boundary currents and equatorial currents.

WBCs are narrow, fast flowing currents that follow the continental slope on the west side of the ocean basin. The WBCs influence the flow well below the surface layer, and separate from the coast continuing out to sea in a narrow jet. These narrow jets usually develop meanders as a result of instabilities in the current and variations in the bottom topography. The exact reason for the separation of these currents is still unknown and is probably related to a number of different factors.

WBC are very important as they result in a large heat transfer from the warm equatorial waters to higher latitudes and as a result modulate the local climate on the adjacent land mass. The most well known example of a WBC is the Gulf Stream in the North Atlantic, which maintains the relatively warm and wet temperate climate of Great Britain and coastal northern Europe. There are two major WBCs in the subtropical gyres of the Pacific. These are the Kuroshio in the north Pacific gyre, and the EAC in the south Pacific gyre. Changes in these WBCs would have a large impact on the local climate of the adjacent landmass.

Eastern boundary currents are often associated with coastal upwelling. Compared to the WBCs, the flow along eastern boundaries is usually shallow, broad, diffuse and slow. This, however, breaks down for currents in close proximity to the coast. Equatorward longshore winds form along the coast and the Ekman transport produced is directed offshore, lowering the sea surface. A corresponding landward horizontal pressure gradient is produced in a band $\sim$100 km wide and generates geostrophic flow towards the equator. The water removed from the coast is resupplied from below in the form of upwelling of colder, nutrient rich waters in a narrow region along the coast. The most impressive coastal upwelling system is the Peru/Chile Current which stretches from 43°S to the equator, where it merges with the equatorial upwelling system in the EEP.

The equatorial current systems are more complex and have only been revealed by detailed field observations, as this region of the world is relatively devoid of shipping traffic and the wind field provides only limited information about the surface currents. The NEC and SEC are wind driven westward flowing currents. Both these currents respond quickly to variations in the wind field, which is strongly seasonal, reaching their greatest flows in the winter of their respective hemisphere when the trade winds are strongest (e.g. the SEC is strongest in August when it reaches speeds of 0.6 m/s).

The two main eastward flowing currents are the Equatorial Undercurrent (EUC) and the North Equatorial Counter Current. The EUC is a swift ribbon of water that flows at 1.5 m/s along the equator, averaging 200 m in thickness and 400 km in width. In the west the core depth of the current is 200 metres below sea level (mbsl) but it rises to 40 mbsl in the east. The EUC forms as a result of the pressure gradient caused by the piling up of the warm surface waters in the west by the trade winds. This results in the sea surface

in the Philippines being 0.5 m higher than the sea surface along the Central American coast. The upward slope of the sea surface to the west produces a downward slope of the thermocline. The EUC flows below the surface currents accelerating down the pressure gradient in the thermocline until friction between the EUC and the surrounding water prevents further acceleration and it reaches steady state.

The EUC is related entirely to the Southern Hemisphere circulation and is primarily sourced from the deeper layers of the SEC (*Tomczak and Godfrey*, 1994). The surface layers of the SEC contribute to the eastward North Equatorial Counter Current, but only during June to September. The rest of the year the North Equatorial Counter Current surface flow is suppressed by the Australasian northwest monsoon system. All these equatorial currents can vary annually, as well as seasonally. They can also alter dramatically during an El Niño event, when evidence suggests the EUC disappears completely (*Tomczak and Godfrey*, 1994).

Subtropical mode waters (STMW) lie between the top of the thermocline and base of the surface water. These STMW, like other mode waters, are formed at the edge of the WBCs by wintertime mixing and cooling prior to re-stratification during the summer. A salinity maximum coincides with the maximum STMW thickness of 120 m (*Roemmich and Cornuelle*, 1992). These STMW may also contribute to the EUC, evident from their similar salinities (*Tsuchiya et al.*, 1989; *Roemmich and Cornuelle*, 1992).

The thermocline and intermediate waters follow the surface wind driven circulation of the subtropical gyres. The formation of thermocline waters are poorly understood. Some are thought to form as a result of convective sinking of high salinity dense surface waters caused by high evaporation in the tropics. While others are hypothesised to be caused by the subduction of high salinity waters during late winter as a result of Ekman layer convergence along the Subtropical Front (STF) (*Tomczak and Godfrey*, 1994). In the Pacific the thermocline waters exhibit a salinity maximum, but display a wide range of temperature and salinity characteristics, which allow them to be subdivided into six water masses covering the different geographical regions (*Tomczak and Godfrey*, 1994).

Intermediate waters are distinguished by their salinity minimum around 600-1000 mbsl. The intermediate water in the Southern Hemisphere subtropical gyre is called the Antarctic Intermediate Water (AAIW). This is primarily formed in the southeast Pacific, just off the coast of South America, associated with the formation of Subantarctic Mode Water (SAMW). It forms along the Subantarctic Front (SAF) due to overturning of the winter mixed layer of the Antarctic Surface Waters (AASW) (*McCartney*, 1977)(Figure 1.10). The SAF is a region of significant wind mixing and high precipitation which give the AAIW its distinct characteristics of high oxygen and low salinity. Once subducted, the AAIW spreads north with its core descending to a depth of ∼1000 mbsl. North Pacific Intermediate Waters (NPIW) form in the northwest Pacific along the Kuroshio and Oyashio Front (*Talley*, 1993). It is formed by the mixing of a combination of deeper waters and does not outcrop at the surface. It has very low salinities, but also lower oxygen levels than its Southern Hemisphere counterpart, the AAIW. In the past the intermediate

waters of the equatorial region have been considered either an extension of the AAIW or the NPIW or a combination of the two. The modern intermediate waters of the Pacific are a primary focus of this thesis and are discussed in Part I, Chapters 3 and 4.

Antarctic Bottom Water (AABW) flow is restricted to many of the deep Pacific Ocean basins as a result of topographic restrictions in the ocean (Figure 1.7). There are three main routes of AABW into the south Pacific; east of Australia into the Tasman Sea, east of New Zealand, and east of the East Pacific Rise (∼110°W). The Tasman Sea route is blocked by topography at 20°S preventing the AABW from entering the Coral Sea to the north, and the East Pacific Rise route is also blocked at 40°S by the presence of the Chile Rise. The southeast basins of the Pacific are therefore not affected by the AABW.

The main distribution of AABW into the Pacific Basin is primarily to the east of New Zealand, where the AABW spreads slowly north eventually entering the northwest Pacific through the Samoa Passage at ∼10°S, ∼169°W. The bottom waters of the northeast Pacific are finally renewed by easterly flow from the northwest. This northeast region of the Pacific is where the oldest waters are found. Radiocarbon ages indicate that it is at least 1000 years since they were last in contact with the atmosphere (*Broecker and Peng*, 1982).

No new deep water is formed in the north Pacific, unlike the north Atlantic, because of low surface salinities. These low surface salinities prevent the formation of deep water from winter mixed layer overturning. Very old "Pacific Deep Water" (PDW) is present between 1000 and 3000 mbsl in the north Pacific. The PDW doesn't contribute significantly to Pacific circulation and its properties are determined by the slow mixing of AABW, intermediate waters and remnants of North Atlantic Deep Water (NADW). There is no exit for the north PDW and therefore it must eventually upwell into the overlying intermediate waters (*Tomczak and Godfrey*, 1994).

At similar depths of 1500 to 3000 mbsl in the south Pacific, NADW is evident as a salinity maximum at around 2000 mbsl. This has been transported by the Antarctic Circumpolar Current (ACC), through the Southern Ocean, and enters the Tasman Sea and the main south Pacific basin to the east of New Zealand. This deep water mass between the intermediate waters and the AABW is often called the Circumpolar Deep Water (CPDW) in the south Pacific (Figure 1.10).

1.3.2 Oceanography of the Southwest Pacific

In this thesis, the "southwest Pacific" refers to the Coral Sea and Tasman Sea. The broad ocean circulation in the Coral Sea and Tasman Sea is highlighted in Figure 1.11. Two water column profiles from the Tasman Sea and Coral Sea, (locations shown in Figure 1.11), illustrate how water masses vary with depth (Figure 1.12). The main surface current in this region is the EAC which is the WBC of the south Pacific gyre. The EAC is sourced from the southern arm of the SEC which bifurcates on collision with the Queensland Plateau at ∼18°S. The northern arm of the EAC is trapped against the Queensland and Papuan boundaries and directed northward to form the New Guinea

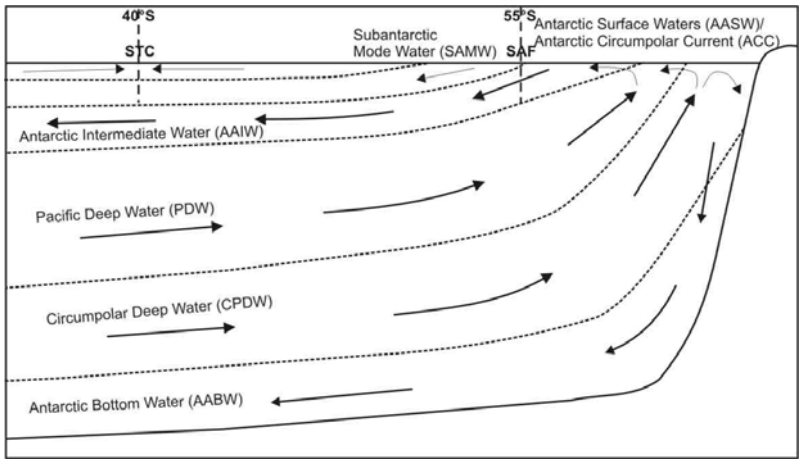

Figure 1.10: Schematic diagram of the water masses at different depths in the Southern Ocean which influence the south Pacific. Antarctic Bottom Waters (AABW), Circumpolar Deep Waters (CPDW), the Pacific Deep Waters (PDW), Antarctic Intermediate Waters (AAIW) forming from the Antarctic Surface Waters or Antarctic Circumpolar Current at the Subantarctic Front (SAF). Also the Subantarctic Mode Waters (SAMW) which from north of the SAF. The Subtropical Convergence (STC) is also shown which is where some of the thermocline waters are formed by subduction.

Coastal Undercurrent (NGCUC) eventually exiting the region through the straits east of Papua New Guinea (*Andrews and Clegg*, 1989). Some of the northerly flow is rerouted south down the Queensland Trough and joins the southern arm of the EAC which continues along the east coast of Australia. At ∼32°S the surface layers of the EAC separate from the coastline, but continue south before retroflecting north and flowing out to sea at ∼34°S in a series of meanders forming the Tasman Front (*Andrews et al.*, 1980; *Ridgway and Dunn*, 2003). This flow continues across the Tasman Sea and around the north island of New Zealand. The subsurface layers and several eddies of the EAC continue south in the Tasman Sea (*Ridgway and Godfrey*, 1994; *Sokolov and Rintoul*, 2000). The dynamics of the EAC will be discussed further in Chapter 7.

STMW are formed at the edge of the WBCs and therefore are found in the southwest Pacific associated with the EAC. The STMW show a thermostad of 15-19°C. A salinity maximum (>35.5‰)(Figure 1.12) coincides with the maximum STMW thickness of 120 m in the southwest Pacific (*Roemmich and Cornuelle*, 1992). The formation and thickness of the STMW in the southwest Pacific varies substantially on an annual basis depending on the strength of the SEC and EAC.

There are two distinct thermocline waters present in the southwest Pacific. The main thermocline water is the Western South Pacific Central Water. This is thought to form at the Subtropical Front (STF) between Tasmania and New Zealand as a result of late winter Ekman convergence causing anticyclonic gyres which lead to subduction (*Tsuchiya*, 1981). The waters being subducted are not denser than the waters below, therefore, the subducted water is injected into the central water mass following an isopycnal surface spreading towards the tropics. The exact location and timing of the Western South Pacific Central Water formation, though, has yet to be identified (*Tomczak and Hao*, 1989). The

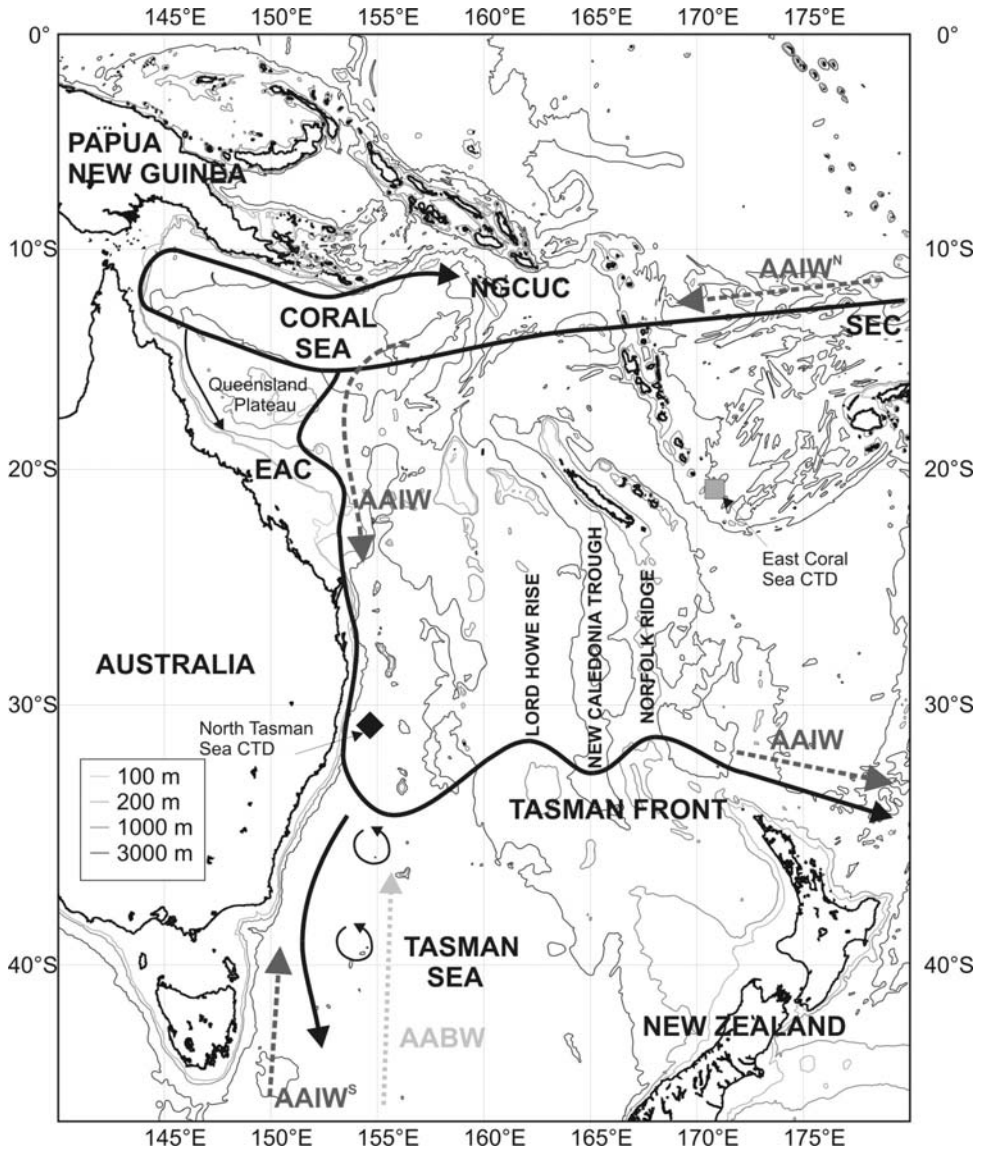

Figure 1.11: The topography in the Tasman Sea and Coral Sea, with the surface water circulation of the East Australian Current (EAC) and the New Guinea Coastal Undercurrent (NGCUC)(black line). Also highlighted are the two arms of the Antarctic Intermediate Water (AAIW) circulation (grey dashed lines). The main source of AAIW^N enters from the northeast Coral Sea, and a second source of AAIW^S enters from the southwest Tasman Sea. Antarctic Bottom Waters (AABW) also enter through the south Tasman Sea (light grey dotted line), however their flow north is blocked by topography at 20°S. The location of the CTD profiles displayed in Figure 1.12 are shown by a black diamond (north Tasman Sea) and grey square (east Coral Sea). Bathymetric contours at 200, 1500 and 3000 mbsl. Adapted from *Tomczak and Godfrey* (1994).

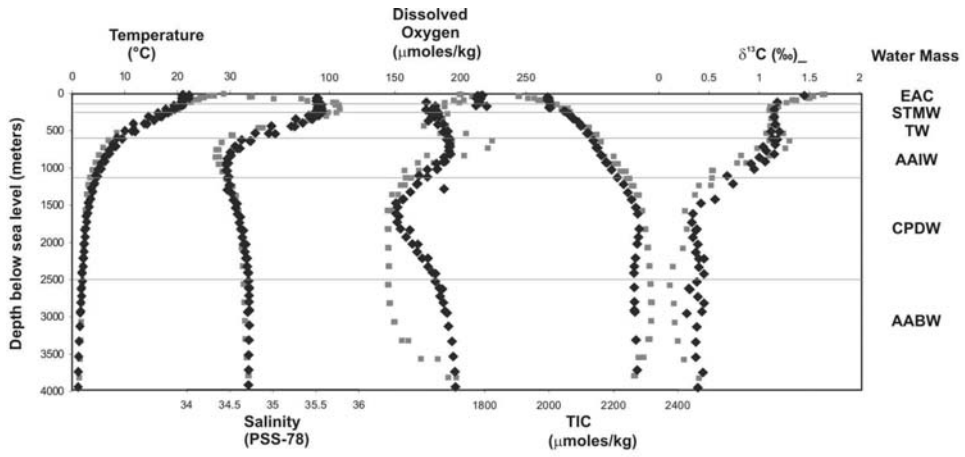

Figure 1.12: Vertical water profiles of temperature, salinity, dissolved oxygen, Total Inorganic Carbon (TIC) and $\delta^{13}C$ of the TIC from two locations (black diamonds - north Tasman Sea, grey squares - east Coral Sea shown in Figure 1.11. The different water masses are separated into the East Australian Current (EAC), the Subtropical Mode Water (STMW), thermocline waters (TW), Antarctic Intermediate Water (AAIW), Circumpolar Deep Water (CPDW) and Antarctic Bottom Water (AABW). Data from WOCE P11s and P21.

other thermocline water is the South Pacific Equatorial Water, which is separated from the Western South Pacific Central water by a frontal zone at 15-20°S in the Coral Sea (*Tomczak and Hao*, 1989). This northern variety has very high salinities and is thought to originate from the tropical central Pacific.

The AAIW is clearly evident throughout the Coral Sea and Tasman Sea by its distinctive salinity minimum. The AAIW enters the region via two sources (Figure 1.11). The southern, minor, slightly higher salinity source (Figure 1.12) flows from the Southern Ocean between Tasmania and New Zealand. The major source of AAIW enters from the northeast Coral Sea, part of the main subtropical gyre. The primary exit for the AAIW follows a similar path to the EAC, along the Tasman Front around the north of New Zealand.

Deep-waters, below the AAIW, enter the Tasman Sea basin from the south and are restricted from leaving the basin in the north by bathymetric constraints at ∼20°S (except for a narrow passage; Figure 1.11). Therefore the deep waters in the Coral Sea display different geochemical profiles to those found in the Tasman Sea. This is particularly evident from the dissolved oxygen concentrations in the CTD profiles below 1750 m (Figure 1.12). In the Tasman Sea there are two distinct deep-water masses, a relatively shallow CPDW and deeper AABW. The CPDW has higher temperatures (2-4°C) and is lower in dissolved oxygen concentrations than the AABW. The CPDW is often separated into upper and lower units (*Park et al.*, 1993), which are distinguished by the oxygen minimum and nutrient variations determined by the deep-water contributions, including the NADW, PDW and Indian deep waters. Below 2500 mbsl, the AABW in the Tasman basin is relatively uniform suggesting a single southern source with limited mixing between the AABW and overlying waters.

Chapter 2

Methods

2.1 Part I - Modern Oceanography

Water data was collected during a series of cruises in the Pacific in the early to mid 1990's as part of the World Ocean Circulation Experiment (WOCE). The overall goal of the WOCE program was to generate a data set of sufficient density and precision to determine the physical properties and circulation of the global ocean. Stations were positioned every $\sim 0.5^{\circ}$ apart along each of the latitudinal or longitudinal cruise tracks and conductivity, temperature, depth (CTD) profiles were taken at each station, as well as discrete water samples from the entire water column. These water samples were measured for temperature, salinity, oxygen, nitrate, nitrite, silicate and phosphate and a subset were measured for chlorofluorocarbons (CFC's), ^{3}H, ^{3}He, $\delta^{13}C$, $\Delta^{14}C$, total inorganic carbon (TIC) and alkalinity (*Key*, 1996).

Nine geochemical tracers were primarily used in Part II of this thesis (salinity, oxygen, phosphate, nitrate, silicate, $\delta^{13}C$, $\Delta^{14}C$, TIC and alkalinity). These tracers were used to specifically study the properties of the intermediate waters along meridional and latitudinal WOCE cruises in the north and south Pacific. The cruises, from which these data were utilised, are outlined in Chapters 3 and 4.

The main measurements used in the paper are from the analyses of bottled samples collected from different depths and publicly available on the WOCE Hydrographic Program Office web site (http://whpo.ucsd.edu/index.htm). Details of the methods, personnel and laboratories used for each analysis are also available from the web site. Several papers have been published analysing the accuracy and comparisons of the carbon data measurements between different transects (*Lamb et al.* (2002), for TIC and alkalinity; *Key et al.* (1996); *Stuiver et al.* (1996), for $\Delta^{14}C$). No corrections to the data have been made for this synthesis of results, as the error range is smaller (e.g. $\pm$ 3 μmole/kg for TIC, $\pm$ 5 μmole/kg for alkalinity, *Lamb et al.* (2002)) than the overall range of the data set for each water mass.

Using these data sets, a range of calculations were also used to determine other parameters such as potential density, and Apparent Oxygen Utilisation (AOU). The equations

for these calculations and others referred to in the text can be found in Appendix C and D.

2.2 Part II - Palaeoceanography

Cores were taken on the Research Vessel Franklin 1/97 Cruise by Dr Bradley Opdyke as part of a coring transect collecting cores from the northern, central and southern Great Barrier Reef (GBR) and south to the Lord Howe Rise. A series of six gravity cores were collected from the Capricorn Channel in the southern GBR from a water depth range of 166 mbsl to ∼3000 mbsl. The main results from these Capricorn Channel cores are outlined in Chapter 5.

2.2.1 Sampling and Sieving

The cores were stored in the Geoscience Australia cold store until required in March 2001, when they were transported to the Department of Earth and Marine Sciences cold store at ANU. The cores were opened using a hand held band saw and steel plate and were wrapped in polythene to keep them damp. One half of the core has been kept as an archive and the other half was logged and sampled. Samples were taken at 10 cm intervals (5 cm for GC-12) from the middle of the core to avoid contamination along the edges or on the surface after splitting.

The samples for foraminifera picking were dried out in the oven at 60°C before being re-soaked in distilled water. After re-soaking, the samples were shaken and placed in an ultrasonic water bath to disaggregate the clays, and the muddy liquid was wet sieved through a series of four fine mesh sieves (400 μm, 300 μm, 200 μm and 100 μm.) Once the size fractions within the sample were separated into a series of beakers, the excess water was siphoned off using a syringe before being transferred to drying trays.

After drying, the size fractions were weighed to determine the % of each grainsize in the overall dried sample. This method is not accurate due to wastage during washing and sieving, at various stages and occasional spills. However, it provides an estimate of % grainsize fraction which can be correlated with other analyses like stable isotopes and $CaCO_3$% and imparts clues to the environmental changes within the core.

Foraminifera were picked under a normal reflective light microscope using a picking tray and a small paint brush at a magnification of x 40 for the larger size fractions of >300 μm and >400 μm. Higher magnification was required for the smaller size fractions.

2.2.2 Stable Isotopes

The largest foraminifera for each species were used for isotopic analysis to avoid the variations in $\delta^{13}C$ that have been observed for different size fractions (*Berger*, 1970; *Oppo and Fairbanks*, 1989; *Elderfield et al.*, 2002). The same size fractions were used throughout the core, thereby selecting foraminifera that were representative of a specific water mass. It

is assumed that variations in the stable isotopes of a species of foraminifera reflect changes in a particular water mass between the glacial and interglacial periods. One problem that cannot be discounted, though, is that species may change their depth range as a result of changing water conditions.

Globigerinoides ruber white were initially picked from the 300-400 μm size fraction to establish a chronostratigraphy for each of the cores using the foraminiferal $\delta^{18}O$ isotope record. 10-15 individual white *G. ruber* were hand picked to give a total sample weight of 180-220 μg for isotope analysis. The samples were washed in methanol and ultrasonicated for 30 seconds to remove any surface and internal particles. The samples were analysed at the Research School of Earth Sciences, The Australian National University, using an automated individual carbonate reaction (Kiel) device coupled with a Finnigan MAT-251 mass spectrometer. Samples were reacted at 90°C in 103% orthophosphoric acid. The $\delta^{18}O$ and $\delta^{13}C$ values were calculated as per mil (‰) deviations relative to VPDB, following calibration with the National Bureau of Standards NBS-19 ($\delta^{18}O$ = -2.20‰, $\delta^{13}C$= 1.95‰) and NBS-18 ($\delta^{18}O$ = -23.0‰, $\delta^{13}C$ = -5.0‰). Average standard deviation for a typical 200 μg sample for the standard NBS-19 was 0.05‰. A suite of planktonic and benthic foraminifera from core GC-12 were also analysed for their stable isotopes. Planktonic species *Globigerinoides sacculifer, Globorotalia menardii, Globorotalia truncatulinoides* and benthic genera *Cibicidoides spp.*. These species were all picked from the >400 μm size fraction and between 3 and 10 individuals were analysed in each sample to give a total sample weight of ~200 μg. For more details about the foraminifera analysed see Appendix E and the species specific isotopic fractionation and corrections are discussed in Chapter 6 .

The chronostratigraphy of the core and the construction of an age model were initially based on correlation of the $\delta^{18}O$ with the SPECMAP curve (Figure 1.6, *Martinson et al.* (1987). This was used to pick appropriate sample depths for AMS radiocarbon dates from a selection of the cores.

2.2.3 Radiocarbon Dating

Radiocarbon AMS dates were run on samples from GC-12 and GC-10 using ~300 individuals (approximately 10-16 mg of $CaCO_3$) *Globigerinoides sacculifer* from the >300 μm size fraction. Samples were rinsed and ultrasonicated in distilled water and dried at 60°C. They were dissolved in 103% orthophosphoric acid and the CO_2 collected under vacuum. The CO_2 was then converted into graphite by reacting with hydrogen over an iron catalyst at 600°C. The reaction occurs in two steps and will only continue to proceed by the second step under these set conditions.

$$\begin{aligned} CO_2 + H_2 &\rightleftharpoons H_2O + CO \\ CO + H_2 &\rightleftharpoons H_2O + C \end{aligned}$$

The iron catalyst was first pretreated to remove any oxidation that may have occurred on the surface of the filings. This is achieved by heating at 400°C under vacuum for an hour

in the presence of H_2 gas. The graphite, once formed, is transferred to small cathodes and run on the AMS.

Once the sample has been analysed it must undergo a series of corrections.

- Contamination - Correction for any contamination or error within the carbon preparation lines and the AMS error.
- Isotope Fractionation - The isotope fractions of carbon have varied through time. During some periods isotope fractionation has enriched or depleted some isotopes relative to the others. This fractionation may occur due to biological "vital effects" or through natural processes. The stable isotope $\delta^{13}C$ is used to compare these variations to the average. If there has been fractionation of the stable isotopes of carbon during the formation of the sample, then there will be a change in the $^{14}C/^{12}C$ ratio of twice the magnitude (since the mass difference is two.) This takes into account that samples will have started off with different ^{14}C concentrations due to natural variations.
- Reservoir Age - The reservoir age for Heron Island, southern GBR, (Latitude 23°S, Longitude 152°E) determined from coral samples (*Druffel and Griffin*, 1999).

^{14}C 484±6 years Historical age 1850
Reservoir age 344±14 years

- True half life - The final correction that should be taken into account is that the true half life of radiocarbon is 5730 years not the original measured value of 5568 years.

These corrections provide a radiocarbon age for the sample. To allow correlation with other data this can be calibrated to a calendar age. Corrections and calibration of the radiocarbon data are outlined in Appendix B.

2.2.4 $CaCO_3$%

A second sample from each depth in the core was dried in the oven and ground up into a fine powder (∼100mm) using a mortar. Approximately 1g of each sample was weighed accurately. 20 ml of ∼1 mol/l HCl was added to the sample, and then heated and stirred until all the carbonate had reacted. The resulting solution was back titrated with 0.5 mol/l NaOH using the Metrohm Ion analysis 716 DMS Titrino series 6.0 to determine the $CaCO_3$%. The error range is ±2%.

2.2.5 X-ray Diffraction

X-ray Diffraction (XRD) was run on a several samples from each of the different cores to determine the main carbonate mineralogy and the primary components of the non-carbonate fraction.

There were two methods of sample preparation. For the majority of samples, the side-packed sample holder was used. Samples were ground in an agate mortar with acetone or ethanol, then dried, and filled into side-packed sample holders. For small samples a low-background holder was required. A very small amount of sample was ground in an agate mortar with acetone or ethanol, applied onto a low-background holder (oriented quartz crystal) with a pipette, and dried.

Powder diffraction data were collected at room temperature with a Siemens D501 diffractometer at the Department of Earth and Marine Sciences, The Australian National University. The diffractometer was equipped with a curved graphite monochromator, a scintillation detector, and CuK_α radiation was used. Scans were recorded in one pass from 2° to 70° $2-\theta$, using a step-width of 0.02° and a scan speed of 1° per minute.

The results were interpreted using the SIEMENS software package Diffracplus Eva (2000), and quantitative estimates were performed using the program Siroquant 2.5.

Several samples were analysed for their clay mineralogy by Franz Gingele. Clays were analysed by adding acetic acid to the <100μm fraction to remove the $CaCO_3$ component. Subsequently it was split into silt (2-100μ) and clay (<2μ) fractions by conventional settling techniques. The clay fraction was analysed by XRD (CoK_α radiation) for the four main clay mineral groups kaolinite, smectite, illite and chlorite following the standard procedures developed by *Biscaye* (1965) and described by *Petschick et al.* (1996). The Contents of each clay mineral group in the sample are expressed as relative percentage (*Gingele et al.*, 2002).